Journal of Applied Electrochemistry

In-Situ Determination of Thickness and Electrochemical Properties of Barrier Oxide Film on Impure Aluminium in Aqueous Solution

--Manuscript Draft--

Manuscript Number:	JACH-D-17-00976R1
Full Title:	In-Situ Determination of Thickness and Electrochemical Properties of Barrier Oxide Film on Impure Aluminium in Aqueous Solution
Article Type:	S.I. : 11th European Symposium in Electrochemical Engineering (ESEE 11)
Keywords:	chronoamperometry; Electrochemical impedance spectroscopy; Cabrera-Mott inverse square law; trace element Pb; passivity; heat treatment; segregation
Corresponding Author:	Kemal Nisancioglu Norges teknisk-naturvitenskapelige universitet Trondheim, NORWAY
Corresponding Author Secondary Information:	
Corresponding Author's Institution:	Norges teknisk-naturvitenskapelige universitet
Corresponding Author's Secondary Institution:	
First Author:	Nils-Håvard Giskeødegård
First Author Secondary Information:	
Order of Authors:	Nils-Håvard Giskeødegård
	Ola Hunderi
	Kemal Nisancioglu
Order of Authors Secondary Information:	
Funding Information:	The Research Council of Norway — Dr. Nils-Håvard Giskeødegård
Abstract:	Lead is present as a trace element (ppm level) in nearly all commercial aluminium alloys. The objective of this work is to investigate the changes incurred by the presence of a small amount (20 ppm) of alloyed Pb and heat treatment on the properties of the barrier oxide in relation to those on pure aluminium, in chloride free acetate buffer. The potential range of interest was -1.1 to -0.1 V vs. saturated Hg/Hg2SO4. The methods used were electrochemical impedance spectroscopy (EIS) and chronoamperometry. The film growth data obtained by chronoamperometry was analysed by use of Cabrera-Mott inverse square logarithmic law. The activation energy for film growth, obtained from this analysis, decreased with increasing heat treatment time and temperature, along with deleterious changes in the electrochemical properties of the oxide, indicating reduced passivity. The steady state data obtained by EIS showed decreasing oxide resistivity with increasing heat-treatment temperature of the samples in the range 300-600°C. These changes were attributed to reduced passivity caused by increased segregation of Pb at the aluminium substrate-film interface.
Response to Reviewers:	Please see the attached file entitled "Comments to Reviewers"

Powered by Editorial Manager® and ProduXion Manager® from Aries Systems Corporation

Manuscript Click here to download Manuscript draft3.docx

In-Situ Determination of Thickness and Electrochemical Properties of Barrier Oxide Film on Impure Aluminium in Aqueous Solution

Nils-Håvard Giskeødegård,[a,*] Ola Hunderi,[b] and Kemal Nisancioglu[a]

a) Department of Materials Science and Engineering, and

b) Department of Physics, Norwegian University of Science and Technology,

7034 Trondheim, Norway

Abstract

Lead is present as a trace element (ppm level) in nearly all commercial aluminium alloys. The objective of this work is to investigate the changes incurred by the presence of a small amount (20 ppm) of alloyed Pb and heat treatment on the properties of the barrier oxide in relation to those on pure aluminium, in chloride free acetate buffer. The potential range of interest was -1.1 to -0.1 V vs. saturated Hg/Hg_2SO_4. The methods used were electrochemical impedance spectroscopy (EIS) and chronoamperometry. The film growth data obtained by chronoamperometry was analysed by use of Cabrera-Mott inverse square logarithmic law. The activation energy for film growth, obtained from this analysis, decreased with increasing heat treatment time and temperature, along with deleterious changes in the electrochemical properties of the oxide, indicating reduced passivity. The steady state data obtained by EIS showed decreasing oxide resistivity with increasing heat-treatment temperature of the samples in the range 300-600°C. These changes were attributed to reduced passivity caused by increased segregation of Pb at the aluminium substrate-film interface.

* Present address: Hydro Primary Metal Technology, Herøya Industripark, 3936 Porsgrunn, Norway

1. Introduction

Lead is present as a trace element at the ppm level in most commercial aluminium alloys, due to its existence in the bauxite ore. The element has been shown to be highly unstable in aluminium because of significant mismatch of the atomic sizes of the two elements, and it segregates by heat treatment first to the grain boundaries and then to the surface by heat treatment [1,2]. The rate of segregation increases with increase in the heat treatment temperature, especially at temperatures exceeding its melting point (328°C). Direct segregation from the surface grains to the surface also occurs. Pb segregates both as a nanofilm and nanosized particles along the oxide-Al metal boundary [3]. Formation of the nanofilm is exacerbated by the formation and inward growth of γAl_2O_3 crystals above 500°C [4,5].

The segregated Pb film contributes to a significant anodic activation of the surface in the presence of chloride in an aqueous environment, as indicated by an appreciable shift in the anodic breakdown potential of the surface in relation to that observed on aluminium with Pb-free surface [5,6]. The particulate segregations do not have a significant effect because they do not wet the aluminium surface. Activation of the surface occurs as a result of undermining of the oxide along the path of the film, as demonstrated on samples heat treated at 600°C by high-resolution field-emission gun scanning transmission electron microscopy (FE-STEM) [3]. It has been difficult to detect film segregation on samples heat treated at lower temperatures or in oxygen free environment. However, electrochemical characterization indicated activation to a smaller degree with decreasing heat treatment temperature, becoming undetectable below 300°C. The activation mechanism in the presence of chloride is not fully clarified. Previous studies of anodic activation of aluminium by Pb have not been

investigated to the extent to which the passivating properties of the barrier oxide *per se* are affected by segregation of the element to the aluminium surface.

The objective of this work is to investigate the utility of the electrochemical methodology of Ref. 7 in studying the modification of the Al metal - barrier oxide and barrier oxide - solution interfaces by external factors, in particular whether electrochemical properties of the oxide, or oxide - metal interface, are significantly affected by the segregation of Pb. For this purpose, a chloride-free acetate buffer solution was used to eliminate the synergistic effect of Cl^-. The methodology [7] involves simultaneous in situ ellipsometry, chronoamperometry and electrochemical impedance spectrometry (EIS). Ellipsometry could not be used presently since heat treatment reduced the specularity of the sample surfaces. While chronoamperometry provided transient data for the film-growth kinetics, EIS was used for extensive steady-state data for potential-dependence of the film properties, as well as for calibrating the transient data between consecutive potential steps.

2. Experimental

Binary aluminium samples, containing about 20 ppm as-weighed Pb, were cast from pure (99.99%) components [3] into 2 cm thick slabs and cold rolled down to 2.2 mm thickness. The samples could not be homogenised, since Pb, even at such low levels used here, has in practice no solubility in Al [2,8]. The samples were metallographically polished through 1 μm diamond paste, and then rinsed in ethanol and dried. They were then heat-treated at 300°C, 450°C and 600°C, from 15 up to 60 minutes. Heat treatment at the lower two temperatures was performed in air. The samples prepared at 600°C were wrapped in aluminium foil, functioning as O_2 filter, and heat-treated in a nearly O_2-free environment,

obtained partly by purging the furnace also with pure argon gas, to avoid formation of thick thermal barrier oxide of gamma alumina [3,5], known to occur at temperatures above 500°C [4].

Choice of Pb composition was based on the amount of earlier data available on the surface properties of this alloy in the range 5 to 50 ppm and heat-treatment temperatures in the range 300°C to 600°C [2,3]. These results show that the heat treatment temperature and the time for heat treatment were more important than the Pb concentration in determining the electrochemical and corrosion properties of the surface. This is due to the fact that the segregated nanofilm, rather than the segregated Pb particles determined these properties.

The experimental apparatus used for EIS and chronoamperometry was identical to the setup presented in the earlier work on pure Al [7,10]. The test electrolyte was a solution of acetic acid and sodium acetate (Na-acetate buffer), 68 g/L NaAc and 7.16 g/l HAc [120 mM], which provided a fixed pH of 5.6, unless specified otherwise. Reagent grade chemicals were used. The experiments were performed at room temperature (22 ± 1°C). The solution was exposed to ambient air. The potentials are reported with respect to Hg/Hg_2SO_4/saturated K_2SO_4 reference electrode.

A Solartron 1286/1260 electrochemical interface/frequency response analyser was used for the chronoamperometry and EIS measurements. For chronoamperometry, the potential was stepped according to the sequence -1.1, -0.7, -0.55, -0.4 and -0.1 V for a given specimen. The current response of the specimen for each step was recorded until a quasi-steady state was observed indicating attainment of a steady-state thickness for the barrier layer corresponding to the applied potential. The current transients were analysed by use of the Mott-Cabrera

inverse square logarithmic growth law as described in Ref. 7. The EIS results, obtained at each steady state between the potential steps were fitted to the impedance model developed in Ref. 7, based on the comprehensive and rigorous model by Armstrong and Edmondson [9], to obtain the equivalent circuit parameters related to the film thickness and conductivity. ZSimpWin (Princeton Applied Research) software was used for the analysis of EIS data.

3. Results

3.1 Growth kinetics

Fig. 1 is a typical plot of the measured current-density transients after several successive potential steps as discussed in the previous section. The main difference between the large and small potential steps was the attained maximum value in current density soon after the step. The peaks increased with increasing potential step, thereby affecting the film-growth rate significantly. The part of the curves immediately following the maxima was used to obtain the oxide growth kinetics. The decrease of current density became monotonic and similar for all potential steps, after 20 - 30 s as the barrier oxide reached its steady-state thickness. At large times, the current transient was governed by factors other than field-assisted growth of the barrier layer, as shown for similar transients for pure Al by comparing the chronoamperomertic data with direct in-situ measurement of oxide thickness transients by ellipsometry [7].

Fig. 2 shows the effect of heat treatment conditions for a selected potential step. The results are compared to those for pure aluminium. The current trends for all transients for a given potential step were similar (please see Ref. 10 for the transients corresponding to the other potential steps of interest). The curves were almost parallel to one another. The current levels

for the AlPb alloys were larger than that for pure Al. The current level in the transients increased a bit from 300 to 450°C. The level of current transients for the samples heat-treated at 600°C were significantly smaller than those for the lower heat-treatment temperatures, becoming quite close to the transients for pure Al, especially for the smaller potential steps [10].

The current-density transients were converted to barrier-film thickness [7] by using the relationship (Faraday's law) [10]

$$\delta(t) = \frac{M_{\mathrm{n}}}{\rho n \mathrm{F}} \int_0^t (i(t) - i_{\mathrm{ss}}) dt \qquad (1)$$

where t is the time elapsed after the potential step, $i(t)$ is the measured current density as a function of time, M_{n} is the molecular weight of the barrier oxide (102 g/mol for Al_2O_3), ρ is its density (3.2 g/cm^3 [11]), n is the number of electrons transferred during oxidation of aluminium (= 6 per mole of Al_2O_3 formed), and F is Faraday's constant. In performing the integration, the leakage current, i_{ss}, was assumed to be constant and equal to the quasi steady-state current density attained after 50 s, at which the current density was presumed to be close to the actual steady state of the barrier-layer thickness [7].

The Cabrera-Mott model was presently used for correlating the data for high-field, thin oxide growth on metals. The time derivative of the oxide thickness can be expressed as [12]

$$\frac{\mathrm{d}\,\delta}{\mathrm{d}\,t} = 2u \sinh\left(\frac{\delta_1}{\delta}\right) \qquad (2)$$

where $\delta_1 = \left(\frac{qaV}{2kT} \right)$, $u = u_0 \exp\left(-\frac{W}{kT} \right) = N\Omega\nu \exp\left(-\frac{W}{kT} \right)$, W is the activation energy for oxidation, k is Boltzmann's constant, N is the surface density of defects, Ω is the volume of oxide ions per metal ion, ν is the jump frequency of the mobile ions, a is the corresponding ionic jump distance between two interstitial points, $E = V / \delta$ is the electric field due to the potential difference V across the barrier oxide, and q is the mobile ion charge.

By integration of Eq. 2, Ghez obtained the expression [13]

$$\frac{\delta_1}{\delta} = -\ln \frac{t+\tau}{\delta^2} - \ln(\delta_1 u) \tag{3}$$

where τ is a constant that can be neglected if it is small compared to t. The derivation is valid only when δ is considerably smaller than δ_1, *i.e.*, for small thicknesses. Eq. 3 is known as the Cabrera-Mott inverse square logarithmic growth law.

Fig. 3 shows a typical Mott-Cabrera plot for the inverse barrier thickness as a function of log (t/δ^2), as calculated from the chronoamperometric measurement shown in Fig. 1 by using Eq. 3. The results showed reasonable straight-line fits in accordance with the Cabrera-Mott inverse square logarithmic oxide growth law, with the possible exception of the data for the potential step -1.1 - -0.7 V. The time ranges, within which the data gave satisfactory fits to straight lines (within a few percent standard deviation), are indicated in the figure. For the large potential step, the inverse-logarithmic region occurred a few seconds after the potential step, while for smaller potential steps the inverse-logarithmic regions started after about 10 seconds, in accordance with the current transients in Fig. 1. Similar data for the other heat-treatment conditions are given in Ref. 10 for the interested reader.

Table 1 shows the slopes obtained by analysis of the chronoamperometric data for all sample conditions and applied potential steps. Table 2 summarises the Cabrera-Mott parameters obtained by fitting the data to Eq. 3 to obtain the parameter *u* and then obtaining parameter *W* from Eq. 2 by assuming $u_o \sim 10^4$ cm/s valid at 22°C [12]. Clear differences between the slopes for pure Al (least negative) and the AlPb alloys were observed. The slope increased slightly in the negative direction with increasing annealing temperature and time applied to the AlPb alloys. A significant negative increase was observed for increase in the annealing temperature from 450°C to 600°C, although the O_2-free condition was used for the higher temperature (Section 2). The slope went through a maximum value with increasing applied potential for the step from -0.55 V to -0.4 V for the AlPb alloys annealed at 300°C and 450°C. These results affected the Mott-Cabrera parameters (Table 2) in the following way:

The δ_1 value, which is the inverse slope, is largest for pure Al. It is significantly smaller for the AlPb alloys, decreasing further with increasing heat treatment temperature and time. The *u* value, which is related to inverse exponential of the activation energy, *W*, and therefore can be considered as a rate constant, is smallest for pure Al. It was many orders of magnitude higher for the AlPb alloys, increasing with increasing heat treatment temperature and time.

The calculated activation energies are plotted in Fig. 4. The activation energy for film formation was largest for pure Al. It was about 50% smaller for the AlPb alloys, decreasing slightly with increasing heat treatment temperature and time. For pure Al, *W* shows a clear dependence on the applied potential, except for the potential step from -1.1 V to -0.7 V. A similar, but reduced, dependence was evident for the AlPb alloy heat-treated at 600°C. In

general, however, the activation energy was quite similar for the alloys treated at 300 and 450°C. The differences observed in this temperature range of heat treatment were within the error limits of the experimental procedure and data analysis, which is estimated to be about 10%. The activation energy did not show a strong dependence on the applied potential in this temperature range either. The abovementioned deviation of the results for the -1.1 V $\rightarrow$ -0.7 V step and for 600°C heat-treated samples will be discussed further in Section 4.

3.2 Steady state results

A detailed coverage of the steady-state results, obtained between successive potential steps, are included since they provided valuable information about the effect of heat-treatment temperature and time. In Fig. 5, the quasi-steady-state current densities, obtained one hour after the potential step, are plotted as a function of applied potential for various values of the heat-treatment temperature and heat-treatment time. These values were significantly larger for the AlPb alloy than for pure Al. The steady-state current density of AlPb sample heat-treated at 600°C was lower than those for the AlPb samples heat-treated at lower temperatures. The difference in the quasi-steady-state current densities of the samples treated at the lower temperatures (300 - 450°C) was not too significant. A small increase in the current density level was observed with increasing heat-treatment temperature (and time) up to 450°C. A small increase in the current density was observed also as a function of increasing potential. The curves showed direct proportionality between the steady-state current density and the applied potential, with nearly the same slope. The curve for 600°C deviated from this proportionality at the most negative potentials.

EIS results were analysed by assuming that the equivalent circuit model, based on the Armstrong-Edmondson model [9], as reproduced in Fig. 6 and shown to apply to the oxide

formed on pure aluminium in acetate buffer [7], is applicable. R_Ω and R_f are the ohmic and polarization resistances, respectively. R_f includes the resistances due to charge transfer at the metal – oxide interface and charge transport through the oxide, and it will be referred to as the "film resistance". The capacitance C includes the electric double layer and barrier-oxide film capacitances in series. The double layer capacitance is normally much larger than the oxide capacitance [11]. The measured capacitance, C, is then nearly equal to the oxide capacitance. The inductance, L, and the related R_L are related to changes in the fluxes of charged species in the barrier layer as determined in a complex manner by their adsorption rates at various interfaces. The significance of the inductive components of the electrochemical interface is outside the present scope and will not be discussed any further.

The thickness of the oxide layer is given by [14,15]

$$\delta = \varepsilon_0 \varepsilon_b \frac{A}{C} \tag{4}$$

where ε_0 is the dielectric constant in vacuum, ε_b is the dielectric constant of the barrier oxide layer, A is the surface area, and C is the capacitance of the oxide. For the barrier layer on aluminium, ε_b is about 10 [16,17].

Fig. 7 shows typical Nyquist plots for AlPb samples heat treated for 40 min at 450°C (Fig. 7a) and for 60 min at 600°C (Fig. 7b). The plot and its analysis in Fig. 7a is representative of all AlPb specimens heat treated at 300 and 450°C [10] and for pure Al [7]. Thus, with the exception of the AlPb sample heat-treated at 600°C, these samples showed nearly ideal semicircular plots, as required by the above model, while the plot for the 600°C sample showed frequency dispersion [18], giving maximum impedance at a lower frequency than for the other samples. Kramers-Kroenig transform analysis indicated reasonable consistency of

the EIS data within the frequencies of interest for the calculation of the capacitance and film resistance with the exception of samples heat-treated at 600°C [10]. These considerations indicate that the proposed model is not valid for the AlPb sample heat-treated at 600°C.

Fig. 8 shows the barrier film thickness, calculated from the film capacitance, as a function of applied potential and heat treatment conditions. In all cases except for the AlPb alloy heat treated at 600°C, the film thickness increased with increasing applied potential. The data for AlPb sample, annealed for 15 min at 300°C, were quite similar to those of pure Al. The film thickness decreased with further increase in the heat treatment time and temperature. The curves in the figure are nearly parallel to one another. The average slope of film thickness - potential plots was 1.16 nm/V, indicating that the data were related to barrier film growth. The samples annealed at 600°C showed anomalous behaviour in relation to the foregoing generalized trends [10].

Fig. 9 shows the effect of applied potential and heat-treatment parameters on the film resistance R_f. This parameter is smaller for all AlPb specimens than that for pure Al. It decreases with increasing heat-treatment temperature and duration with the exception of the samples treated at 450. In the case of 450°C sample, increasing the heat-treatment time from 30 to 60 min seems to give a slight increase in R_f. The effect of applied potential on R_f was very small. There was a tendency for a slight decrease to a minimum from -0.7 to -0.55 V, with a slight increase again with further increase in the potential, similar to the clearer changes for pure aluminium. The R_f for the 600°C increased significantly with increase in the potential, almost reaching the resistance of the untreated pure Al [10].

4. Discussion

It should be recalled from Section 2 that heat treatment of samples at 300 and 450°C was performed in air, while it was performed in oxygen-free environment at 600°C. Moderate growth of the oxide by heat treatment in air is expected in the temperature range 300 - 450°C, based on earlier work on impure Al containing Pb as a trace element, although this was based on *ex-situ* characterisation [5,6]. In the absence of O_2 during heat treatment, such thickening of the film is not expected although the filtering of O_2 from pure Ar by the present approach may not have given a 100% O_2-free gas in the heat-treatment chamber. Apparent film thinning with increasing heat treatment temperature and time, suggested by the steady-state EIS data, can be due to film dissolution when the samples are immersed in the test solution after heat treatment during stabilisation of the surface at the initial potential before the start of the potential steps of the chronoamperometric measurement. Film thinning is also suggested by the corresponding increase in the leakage current and decreasing polarisation resistance with increasing heat-treatment parameters. However, these results can also be related to increasing capacitance and decreasing resistance of the film by increasing Pb contamination [1,2]. The lack of *in-situ* ellipsometry data can be considered as a drawback against a definitive conclusion in this respect.

In addition to the foregoing, the transient results indicate a significant increase in the negative slope of the straight-line fits of data to Eq. 3 and a corresponding significant decrease in the Mott-Cabrera parameters δ_1 and W for the AlPb alloy relative to pure aluminium (Table 2). These parameters further change more moderately, but in the same direction, with increasing annealing temperature and time. W is about 50% smaller for the AlPb alloys, decreasing slightly with increasing heat treatment temperature and time. These results can be regarded as

additional evidence to the conclusion that the passivity of the barrier film decreases as a result of increasing contamination with Pb with increasing heat-treatment temperature and time.

The potential dependence of the relative film thickness (1.2 nm/V) for given heat treatment conditions (except treatment at 600°C) is indicative of growth of barrier oxide film as on pure aluminium [7], independent of Pb segregation. However, the level of Pb contamination affects the absolute thickness relative to that for pure Al. This may be related to the likelihood that the oxide formed is still pure Al oxide with the same composition and structure as on pure Al at molecular scale, while the apparent conductivity of the contaminated oxide is reduced. This is possible if the segregated Pb does not chemically interact with the Al oxide.

Segregated Pb was not visible by scanning electron microscopy (SEM) or FE-TEM for samples annealed at temperatures smaller than 600°C in earlier work [3,5,6]. However, it was detectable by (glow-discharge optical emission spectroscopy (GD-OES) depth profiling and potentiodynamic polarization in chloride solution in the temperature range above 300°C [5,19]. Pb particles as large as 100 nm in diameter, which segregated to the oxide surface during heat treatment at 600°C, became readily observable by SEM and FE-TEM. FE-TEM investigation of samples heat treated in air at 600°C also revealed formation of a nearly continuous Pb-rich film of a few nanometer thickness between the metal surface and the γ-Al_2O_3 crystals growing into the metal from the surface [3,5,6]. In O_2-free environment, Pb segregation in the form of particles, migrating through the unaffected air-formed oxide film to the surface, was also readily visible via SEM analysis of AlPb samples annealed at 600°C [20,21].

The activation energy for film growth, *W*, in the original Mott-Cabrera formulation, does not include the effect of an applied potential, as it should in the present case for film growth in an aqueous solution. Despite this important difference in relation to the classical derivation, the present results, especially for pure Al [7], show high-field assisted barrier-film growth in aqueous solution. For these cases, the effect of applied potential is expected to be incorporated into the activation energy. Thus, *W* shows clear dependence on applied potential (Fig. 4 and Ref. 7). It decreases with increasing potential for pure Al, indicating reduced energy needed (or increase in energetically favourable conditions) for the growth of the barrier layer (anodizing), as expected. For the AlPb alloys, however, the effect of applied potential on *W* is of reduced significance relative to pure aluminium. The film resistance R_f is analogously independent of applied potential for AlPb alloys (with the exception of 600°C-annealed sample) relative to pure Al (Fig. 9). These results can be due to an effect, which counteracts the expected decrease of *W* and analogously expected increase of R_f , with increasing potential for the AlPb alloys. The cause of the observed effect is unclear, other than the likelihood that it is related to Pb segregation. Increasing segregation of Pb into the film and/or at the metal-film interface can be attributed to cause such an effect.

The chronoamperometric data for the potential step -1.1 to -0.7 V do not quite follow the foregoing discussion about the effect of applied potential. It is questionable whether the Mott-Cabrera law is applicable for the measured current transients for this potential step. A possible cause is hydrogen evolution, probably localised to the Pb segregations, which will affect the current transient, although the actual film growth may satisfy the Mott-Cabrera law, as was shown to be the case for pure Al [7]. Another possibility is the oxidation of the Pb particles in this potential range to form soluble Pb^{2+} or a Pb-oxide. The oxide may

moreover exhibit considerably lower electrical conductivity than metallic Pb [22]. Thus, the effect of a secondary reactions and/or change in the electrokinetic properties of the Pb segregations could contribute to the observed anomaly.

The anomalous behaviour of the 600°C-annealed AlPb sample in relation to the other alloys discussed above needs separate evaluation. It is again based on the possible effects of Pb segreation along with film thickening and crystallization, which occur only locally [20,21]. Film thickening and local crystallization may cause reduced leakage current relative to the AlPb samples annealed at lower temperatures. This is still higher than the leakage current for pure aluminium, although it was not heat treated, but is under otherwise identical conditions (Fig. 5). The observed effect may be attributed partly to Pb segregation.

Many of the segregated particles on samples annealed at 600°C under O_2-free conditions are large enough to grow through the oxide on top of the oxide film during heat treatment, while they are still in metallic contact with the aluminium alloy substrate [20]. These nearly spherical Pb-metal sites, although contributing to a small increase in the surface area, are still expected to cause detectable increase in the measured capacitance. Their capacitance (per area) is significantly higher than the film capacitance. In addition, nonuniformity of charge distribution at the surface caused by the metallic Pb particles exposed on a surface covered by a relatively insulating oxide will contribute to the frequency dispersion of the measured impedance. These factors are expected to give significantly increased values to the measured (effective) capacitance and resistance of the electrochemical impedance in relation to the true values. As a result, the results reported for the samples annealed at 600°C can become erroneous.

Kramers-Kroenig transform analysis [10] indicate reasonable consistency of the EIS data within the frequencies of interest for the calculation of the capacitance and film resistance with the possible exception of samples heat-treated at 600°C. Time dependent phenomena during impedance measurement may thus be a factor in addition to nonuniformity of charge distribution. Changes in the electrochemical properties of this alloy (heat-treated at 600°C) with increasing potential can also be interpreted as changes occurring with increasing time of immersion in the test solution. Moreover, passivation of the exposed Pb particles above the reversible potential of Pb oxidation is possibly reflected in the increase exhibited by R_f with increasing potential, approaching the R_f value of pure Al asymptotically with increasing applied potential [10]. Meanwhile, the measured capacitance and calculated film thickness remain relatively unaffected above -0.4 V, as would be expected according to the hypothesis of Pb passivation.

The present results are limited in identification of the exact causes of the observed property changes, whether these can be attributed to the barrier film properties *per se* or modifications occurring at the metal-film interface, such as segregation of a Pb film by heat treatment and chronoamperometric polarization. The results show, however, significant differences in the electrochemical properties of pure Al, AlPb alloy heat-treated at temperatures below 600°C, and the properties of alloy treated at 600°C. While the formation kinetics of the barrier oxide on pure aluminium in the aqueous buffer solution appears to be governed by the Mott-Cabrera high field growth mechanism, analysis of the data for the AlPb alloy becomes increasingly difficult with increasing Pb segregation to the metal surface, into the barrier film and to the film surface, especially in the case of samples annealed at 600°C. In this case, the nature of Pb segregation was documented by SEM in earlier work. For specimens annealed in air, the available GD-OES and potential-controlled electrochemical data suggest segregation

at the metal-oxide interface [5,19]. The present results complement the earlier evidence of Pb segregation at the surface (in the film and/or film-metal interface), which can be summarized as deterioration of the passivity in general for the samples annealed at temperatures smaller than 600°C, relative to that for pure aluminium.

We have presently refrained from using the empirical constant phase element approach for analysing non-ideal EIS data, affected by frequency dispersion, for estimating oxide film thickness. The cause of deviation from ideal behaviour, reflected in the form of frequency dispersion of the impedance data, can be caused by various factors discussed above. Without the availability of a mathematical model, which incorporates these factors [23], one cannot with certainty estimate the thickness of oxide films, which are characterized by in depth and lateral distribution of a segregated trace element, respectively, in the form of nanoparticles in the oxide and nanofilm at the metal-oxide interface.

5. Conclusions

- Analysis of chronoamperometric data by using the Mott-Cabrera inverse-logarithmic growth law indicates faster growth of the Pb-contaminated barrier layer on aluminium in relation to that on pure aluminium. However, the passivating properties of the Pb-contaminated oxide are poorer than the oxide grown on pure Al. These two results are not contradictory to one another in view of a higher dissolution rate expected on the poorer oxide.
- Increasing Pb contamination of the barrier-layer, as a result of heat treatment, causes reduction of oxide thickness in the test solution in relation to the film thickness on pure Al and commensurate with increasing heat-treatment temperature (below 600°C) and time.

- Pb segregation, with the exception of significant particulate segregation by annealing at 600°C, did not affect the expected 1.2 nm/V thickness-potential relationship of the barrier oxide on aluminium.
- Deterioration of passivity relative to pure Al, by Pb segregation for AlPb samples annealed at temperatures as low as 300°C, is in agreement with earlier electrochemical polarization data. These results are in agreement also with earlier GD-OES depth profile data, showing Pb segregation at the oxide - metal interface at such low annealing temperature.
- Reduced deterioration of passivity for the sample heat treated at 600°C in O_2-free atmosphere, despite significant Pb segregation, especially at potentials exceeding the thermodynamic reduction potential of metallic Pb, is attributed to oxidation of Pb.
- The use of indirect chronoamperometric data alone for estimation of film growth rate, due to difficulty in obtaining reliable, simultaneous ellipsometric data in the present study, was a drawback in situations where film growth was affected by complicating factors, such as contamination of oxide film and film-metal interface by Pb and resulting nonuniformity of current distribution, as in the case of samples annealed at 600°C. This factor affected also the reliability of the steady-state EIS data, necessary for the calibration of the chronoamperometric data.

Acknowledgements

This work was supported by The Research Council of Norway.

References

1. Gabrisch H, Dahmen U, Johnson E (1998) Microsc Microanal 4: 286
2. Gundersen JTB, Aytac A, Nordlien JH, Nisancioglu K (2004) Corr Sci 46: 697

3. Anawati A, Graver B, Nordmark H, Zhao Z, Frankel G, Walmsley JC, Nisancioglu K (2010) J Electrochem Soc 157: C313

4. Shimizu K, Furneaux RC, Thompson GE, Wood GC, Gotoh A, Kobayashi K (1991) Oxid Met 35: 427

5. Sævik Ø, Yu Y, Nordlien JH, Nisancioglu K (2005) J Electrochem Soc 152: B334

6. Yu Y, Sævik Ø, Nordlien, JH, Nisancioglu, K (2005) J Electrochem Soc 152: B327

7. Giskeødegård NH, Hunderi O, Nisancioglu K (2015) J Solid State Electrochem 19: 3473-3483

8. Masaki T, editor (1990) Binary Alloy Phase Diagrams. ASM International, Materials Park, Ohio

9. Armstrong RD, Edmondson K (1973) Electrochim Acta 18:937

10. Giskeødegård NH (2016), Barrier Oxide Growth and Dissolution on Aluminium in Aqueous Media. Dissertation, Norwegian University of Science and Technology, https://brage.bibsys.no/xmlui/bitstream/handle/11250/2426386/Nils%20H%C3%A5vard%20Giske%C3%B8deg%C3%A5rd_PhD.pdf?sequence=1

11. Gudic S, Radosevic S, Kliskic M (1996) J Appl Electrochem 26:1027

12. Cabrera N, Mott NF (1948-1949) Rep Prog Phys12:163

13. Ghez R (1973) J Chem Phys 58:1838

14. Vetter KJ (1971) Electrochim Acta 16:1923

15. Bessone J, Mayer C, Jüttner K, Lorenz WJ (1983) Electrochim. Acta 28:171

16. De Wit J, Lenderink H (1996) Electrochim Acta 41:1111

17. Young L (1961) Anodic Oxide Films. Academic Press, New York

18. Jorcin JB, Orazem ME, Pébère N, Tribollet B (2006) Electrochim Acta 51:1473

19. Şenel E, Nisancioglu K (2018) Corr Sci 131:330

20. Sævik Ø, Nordlien JH, Nisancioglu K (2003) ATB Metallurgie, 43(1-2):159

21. Walmsley JC, Sævik Ø, Graver B., Mathiesen RH, Nisancioglu K (2007) J Electrochem Soc 154:C28
22. Darwish A, El-Zaidia E, El-Naass M, Hanafy T, Al-Zubaidi, A (2014) J Alloys Compd 589:393
23. Hirschorn B, Orazem ME, Tribollet B,Vivier V, Frateur I, Musianid M (2010) J Electrochem Soc 157:C452

Table 1. Summary of slopes obtained by analysis of chronoamperometric growth data, by use of Cabrera-Mott inverse square logarithmic growth law.

		Potential Step (V_{Hg/Hg_2SO_4})			
Heat treatment temperature (°C)	Heat treatment time (min)	-1.1 → -0.7	-0.7 → -0.55	-0.55 → -0.4	-0.4 → -0.1
		Slope based on current transient (nm^{-1})			
Pure Al		-0.1	-0.030	-0.034	-0.052
300	30	-0.2	-0.11	-0.089	-0.10
300	60	-0.3	-0.13	-0.10	-0.11
450	15	-0.3	-0.15	-0.12	-0.14
450	40	-0.3	-0.15	-0.12	-0.15
600	60	-0.5	-0.94	-0.15	-3.0

Table 2. Summary of results obtained by analysis of the chronoamperometric data by use of Cabrera-Mott inverse square logarithmic growth law, expressed in terms of the Cabrera-Mott parameters δ_1, u and W.

Heat treatmeant temperature (°C)	Heat treatment time (min)	Potential step (V_{Hg/Hg_2SO_4})											
		-1.1 → -0.7			-0.7 → -0.55			-0.55 → -0.4			-0.4 → -0.1		
		δ_1 (nm)	*u* (nm/s)	*W* (eV)	δ_1 (nm)	*u* (nm/s)	*W* (eV)	δ_1 (nm)	*u* (nm/s)	*W* (eV)	δ_1 (nm)	*u* (nm/s)	*W* (eV)
Pure Al		16	$1.3\cdot10^{-10}$	1.2	77	$5.6\cdot10^{-22}$	1.9	68	$4.3\cdot10^{-18}$	1.7	44	$6.2\cdot10^{-7}$	1.24
300	30	14	$2.5\cdot10^{-6}$	0.97	21	$1.6\cdot10^{-7}$	1.0	26	$3.3\cdot10^{-8}$	1.1	23	$2.4\cdot10^{-6}$	0.97
300	60	8.1	$1.1\cdot10^{-4}$	0.88	18	$4.9\cdot10^{-7}$	1.0	22	$1.3\cdot10^{-7}$	1.1	20	$5.7\cdot10^{-6}$	0.95
450	15	8.6	$1.0\cdot10^{-4}$	0.88	15	$1.9\cdot10^{-6}$	0.98	19	$4.4\cdot10^{-7}$	1.0	17	$2.3\cdot10^{-5}$	0.92
450	40	6.3	$2.0\cdot10^{-4}$	0.86	15	$2.2\cdot10^{-6}$	0.98	19	$5.4\cdot10^{-7}$	1.0	16	$3.5\cdot10^{-5}$	0.91
600	60	4.7	$3.1\cdot10^{-4}$	0.85	2.5	$2.1\cdot10^{-6}$	0.86	1.5	$6.9\cdot10^{-4}$	0.83	0.8	$2.1\cdot10^{-2}$	0.74

Figure Titles

Figure 1. Current density vs. time for AlPb sample heat-treated for 40 minutes at 450°C for successive potential steps (V_{Hg/Hg_2SO_4}) specified in the legend.

Figure 2. Current density vs. time for AlPb sample after potential step from -0.4 to -0.1 V_{Hg/Hg_2SO_4} for different heat treatment temperatures and periods. The results are compared with the corresponding transient for untreated pure Al

Figure 3. Inverse thickness, calculated from the current transients, as a function of log (t/δ^2) for potential steps (V_{Hg/Hg_2SO_4}) specified in the legend. The sample was heat treated for 40 minutes at 450°C. The slopes of the straight line fits in nm^{-1} and the time ranges of data used for the straight line fits are included. Similar correlation for untreated pure Al is shown for comparison.

Figure 4. Activation energy as a function of applied potential *U* (V_{Hg/Hg_2SO_4}) for various heat treatment times and temperatures. Results for pure aluminium obtained by the same methodology are included for comparison.

Figure 5. Quasi-steady-state current density vs. applied potential *U* (V_{Hg/Hg_2SO_4}) for AlPb samples heat treated for various periods at various temperatures and for pure Al.

Figure 6. a) Equivalent circuit model for pure aluminium covered by its barrier oxide in aqueous solution and b) the corresponding Nyquist diagram.

Figure 7. Typical measured EIS spectra (Nyquist plot) for two heat-treatment conditions for AlPb alloy: a) 40 min at 450°C, b) 60 min at 600°C. Measurements were performed at an applied potential of -0.1 V_{Hg/Hg_2SO_4}.

Figure 8. Barrier film thickness vs. applied potential *U* (V_{Hg/Hg_2SO_4}) for heat-treated AlPb samples and for pure Al.

Figure 9. Oxide resistance vs. applied potential *U* (V_{Hg/Hg_2SO_4}) for heat-treated aluminium samples and for pure Al.

Figure 1

Click here to download Figure fig1.tif

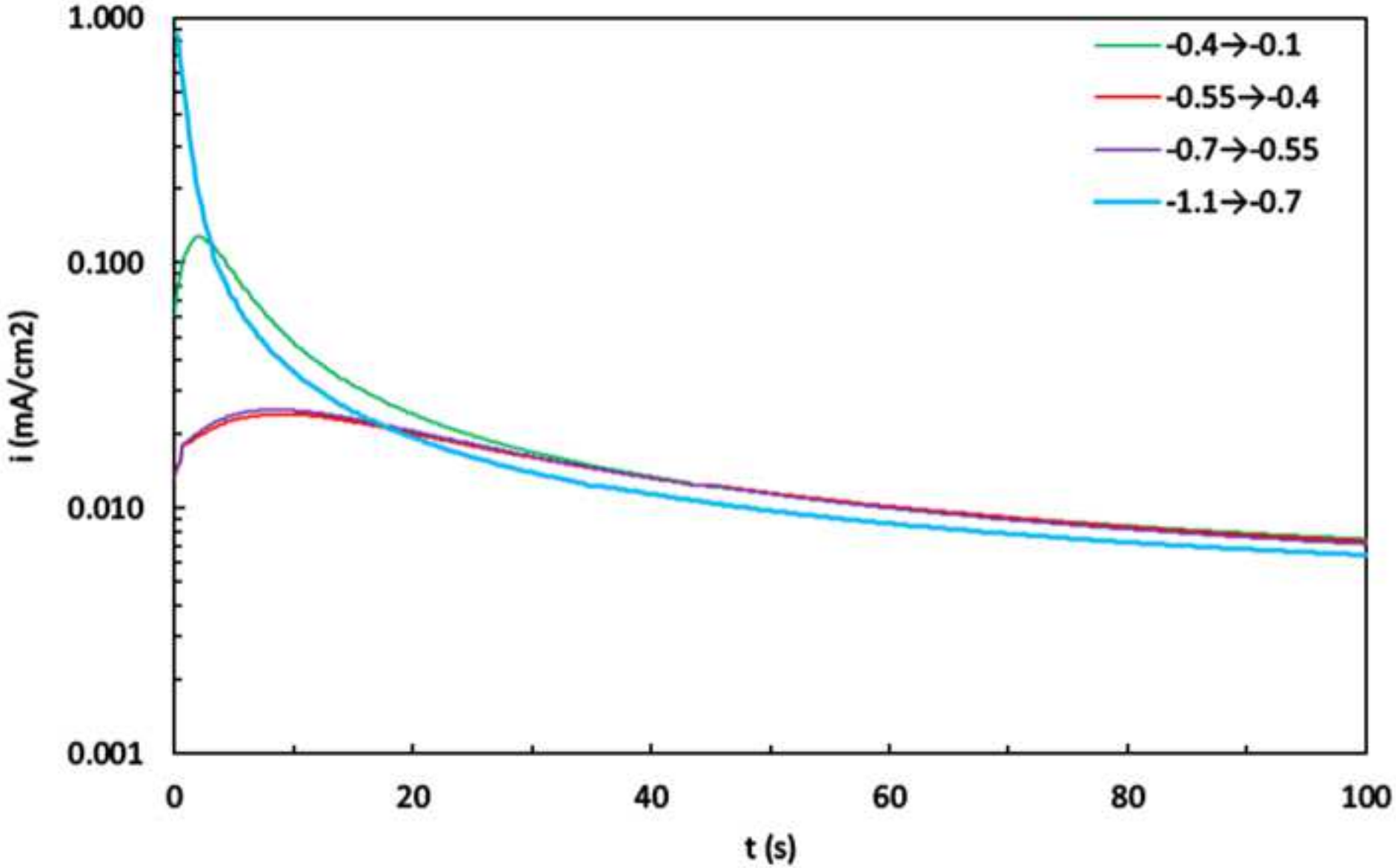

Figure 2

Click here to download Figure fig2.tif

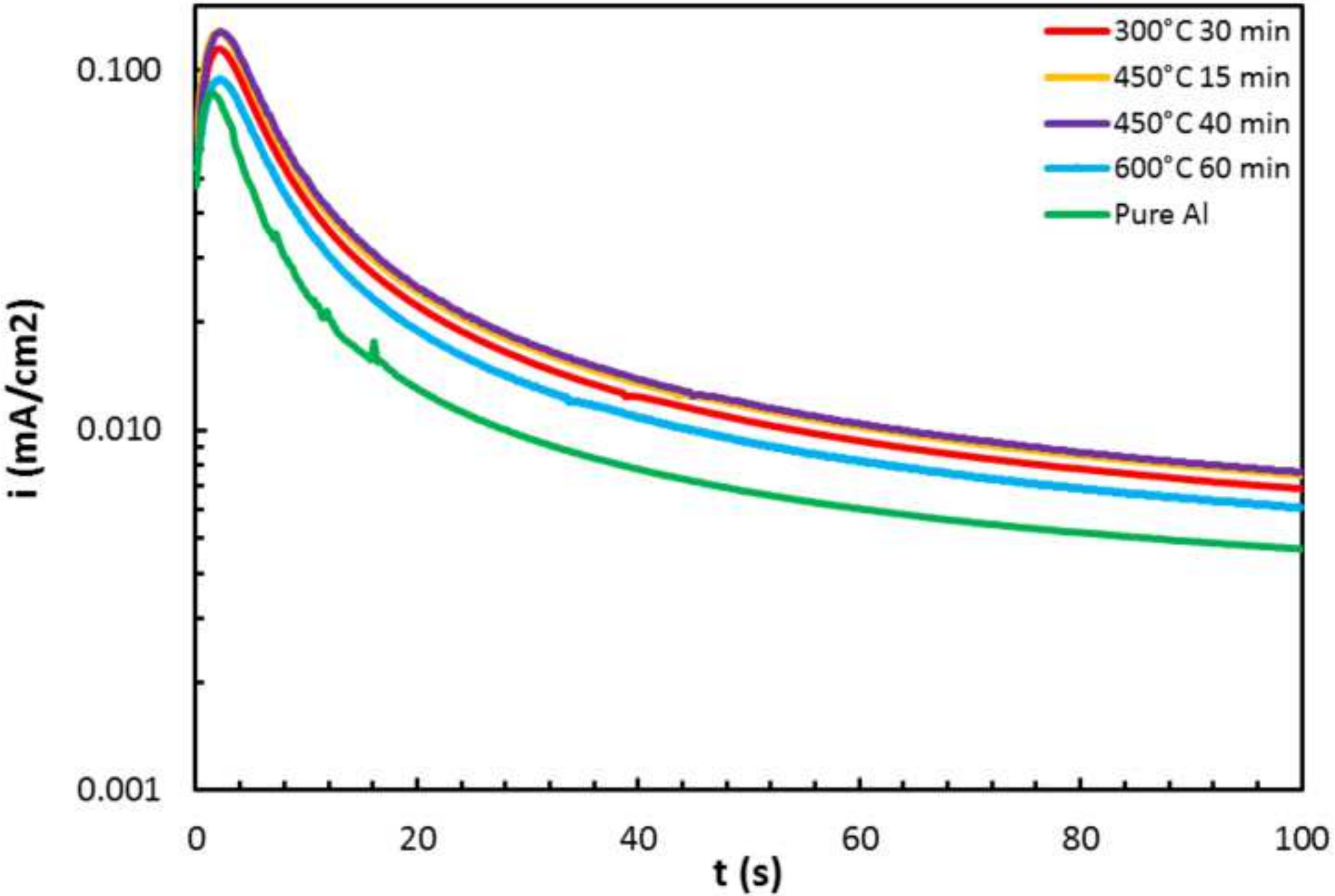

Figure 3

Click here to download Figure fig3new3.tif

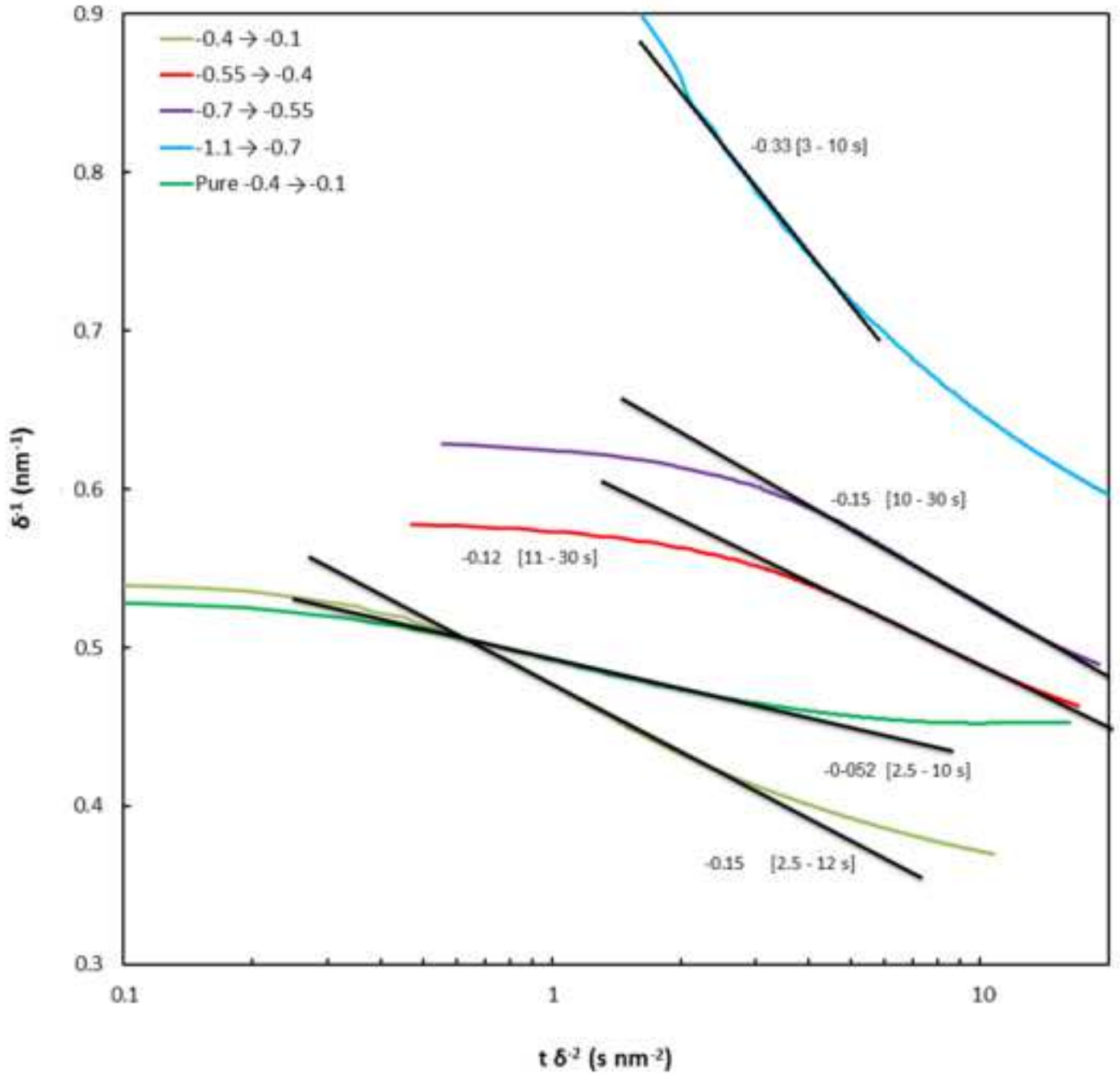

Figure 4

Click here to download Figure fig4 new.tif

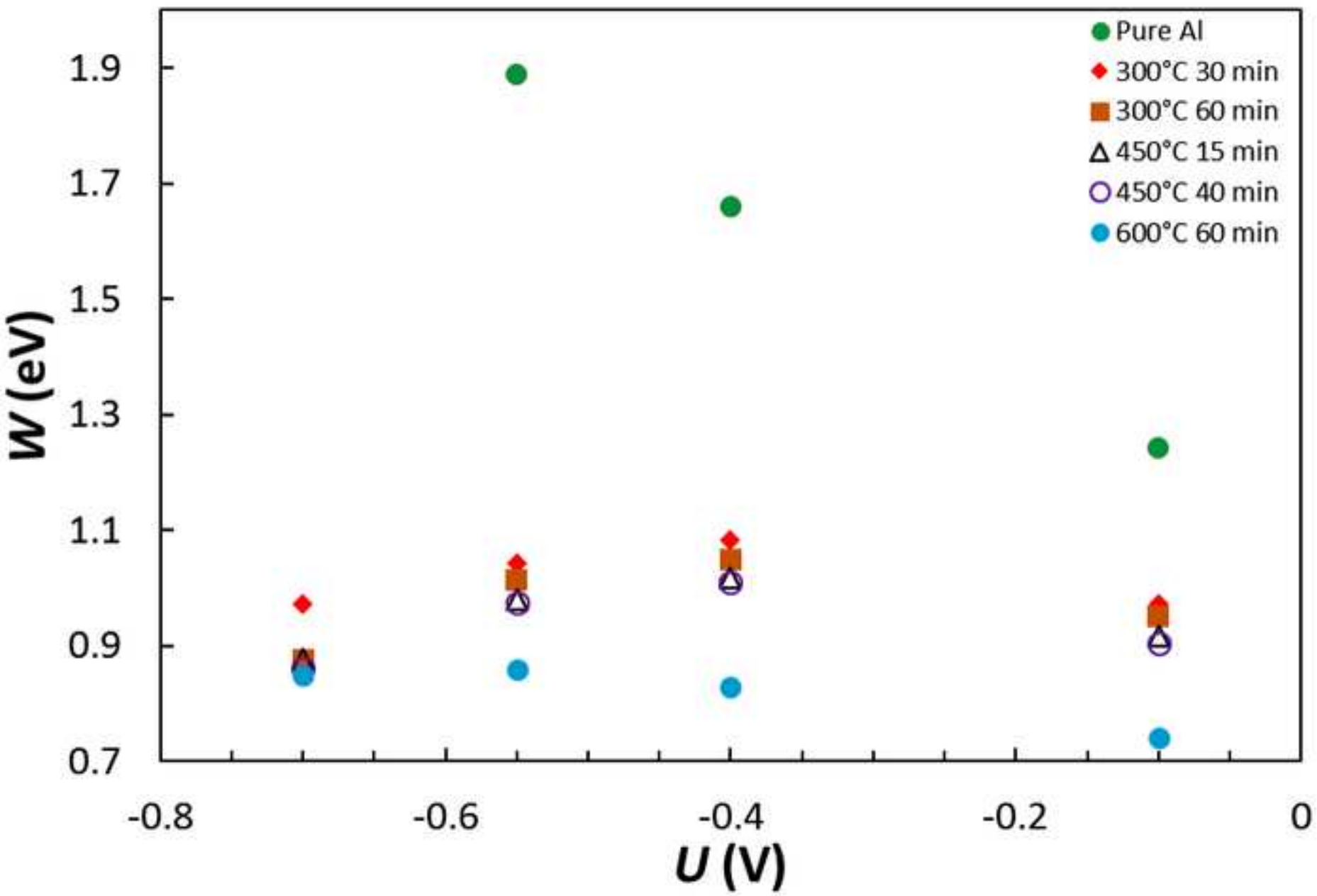

Figure 5

Click here to download Figure fig5 new.tif

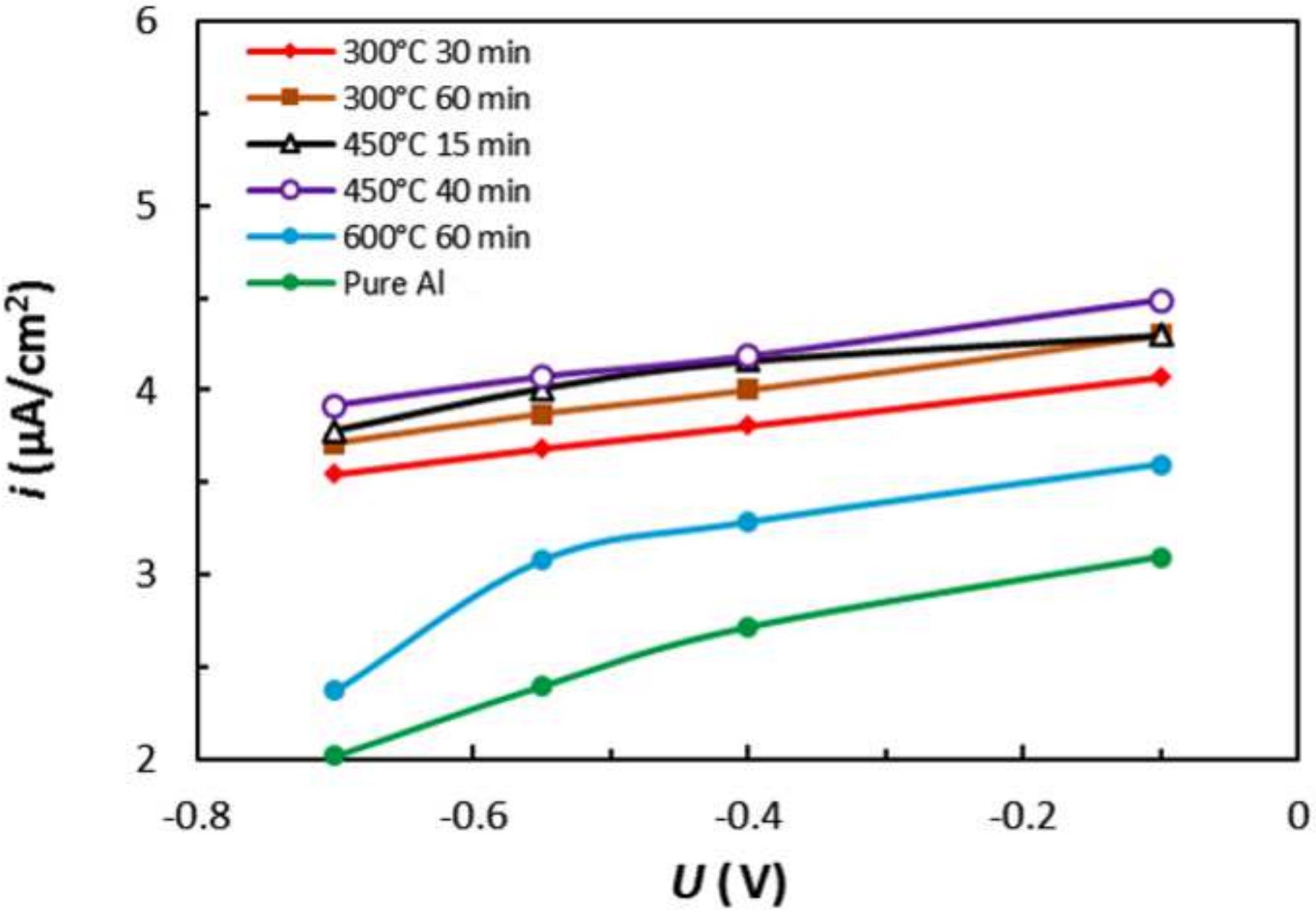

Figure 6a

Click here to download Figure fig6a.tif

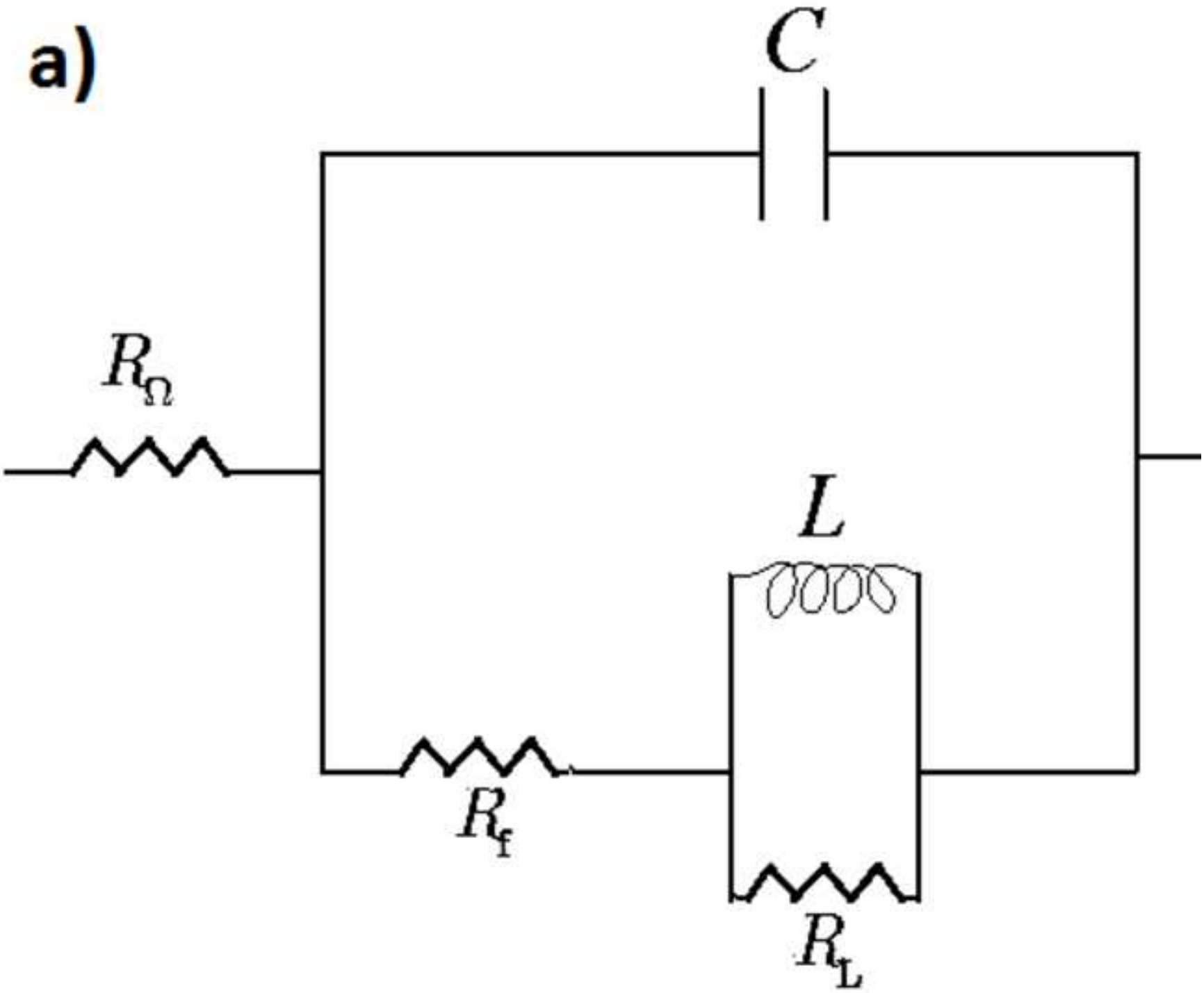

Figure 6b

Click here to download Figure fig6b rev.tif

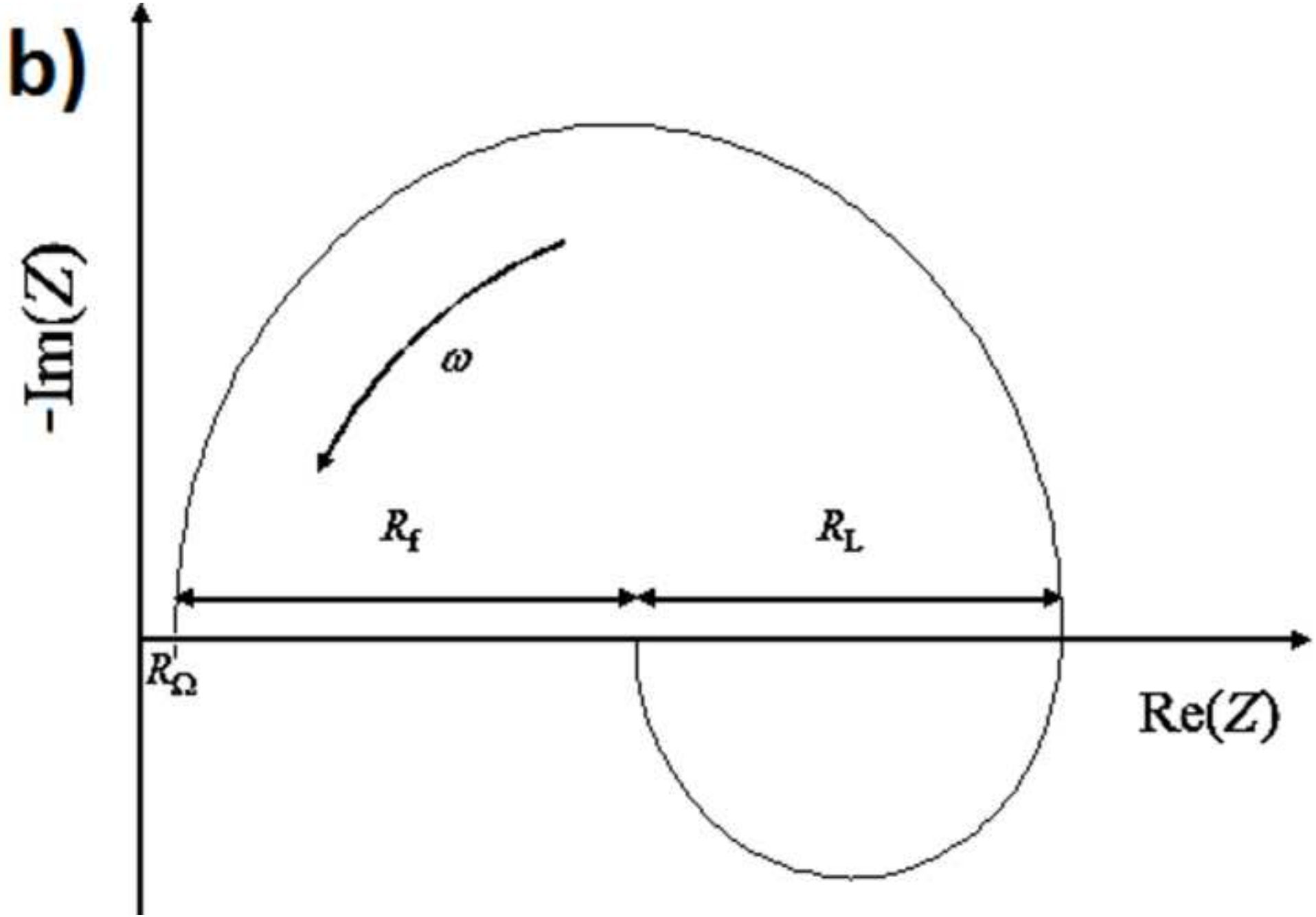

Figure 7a

Click here to download Figure fig7a new4.tif

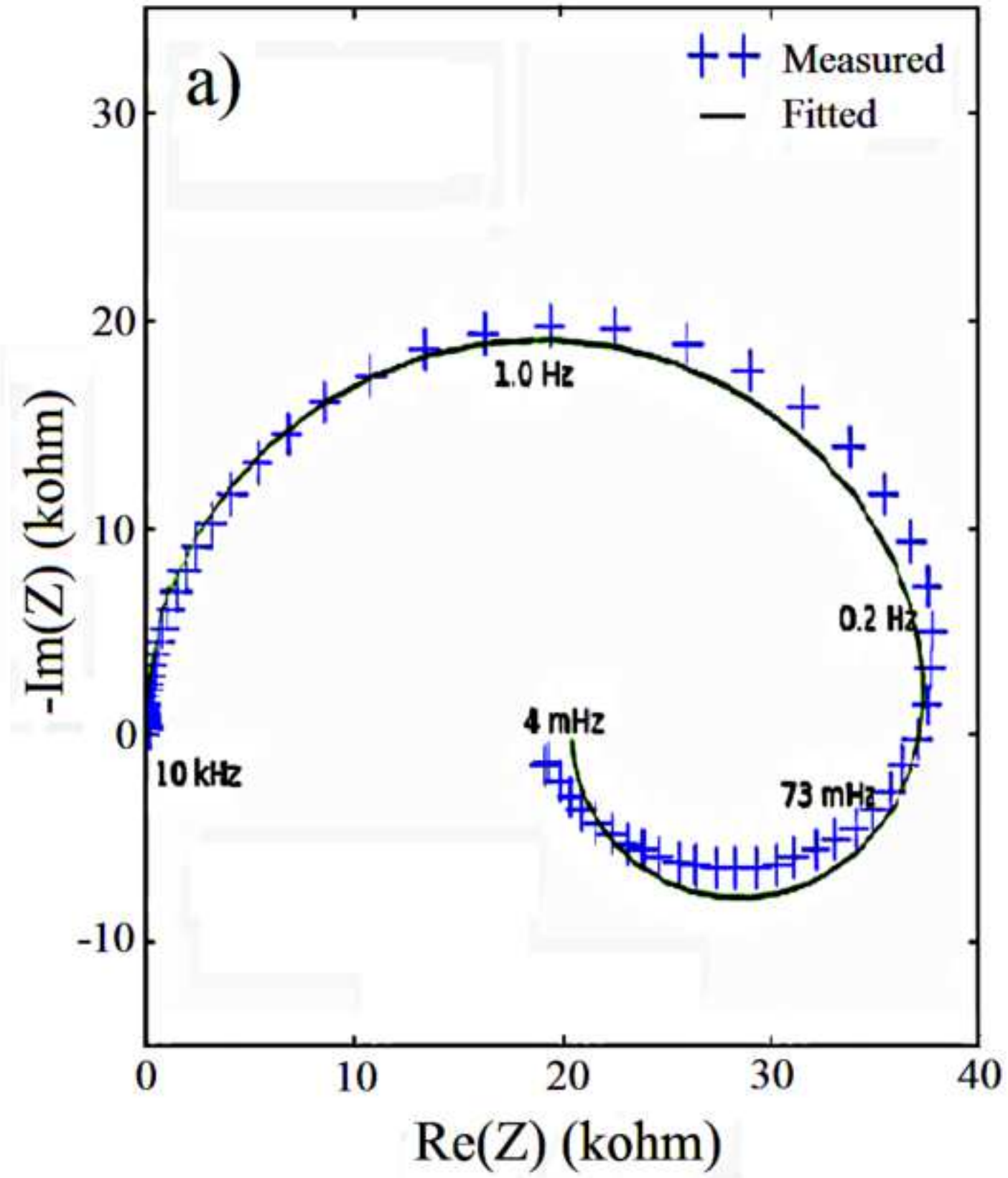

Figure 7b

Click here to download Figure Fig7b new1.tif

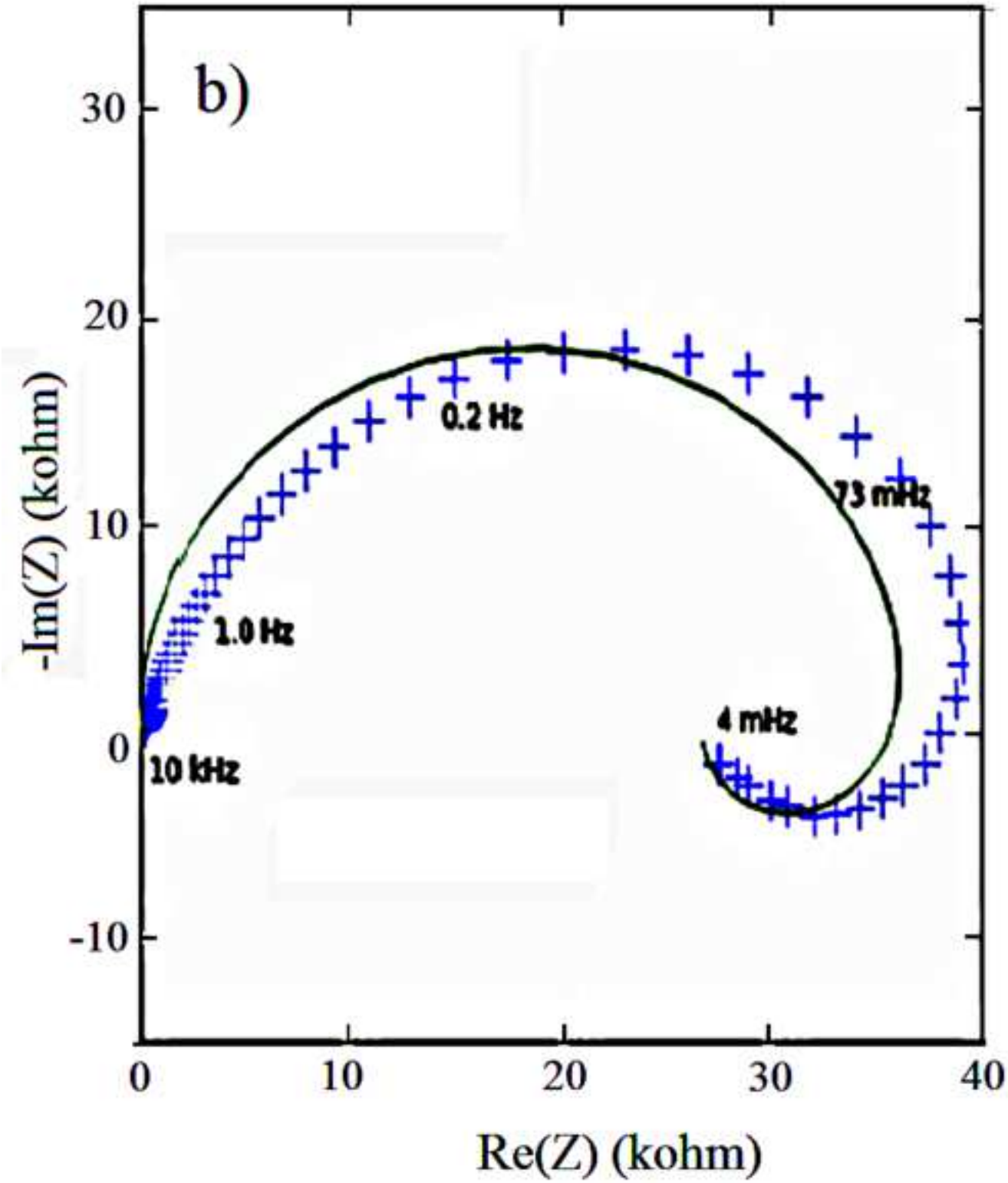

Figure 8

Click here to download Figure fig8.tif

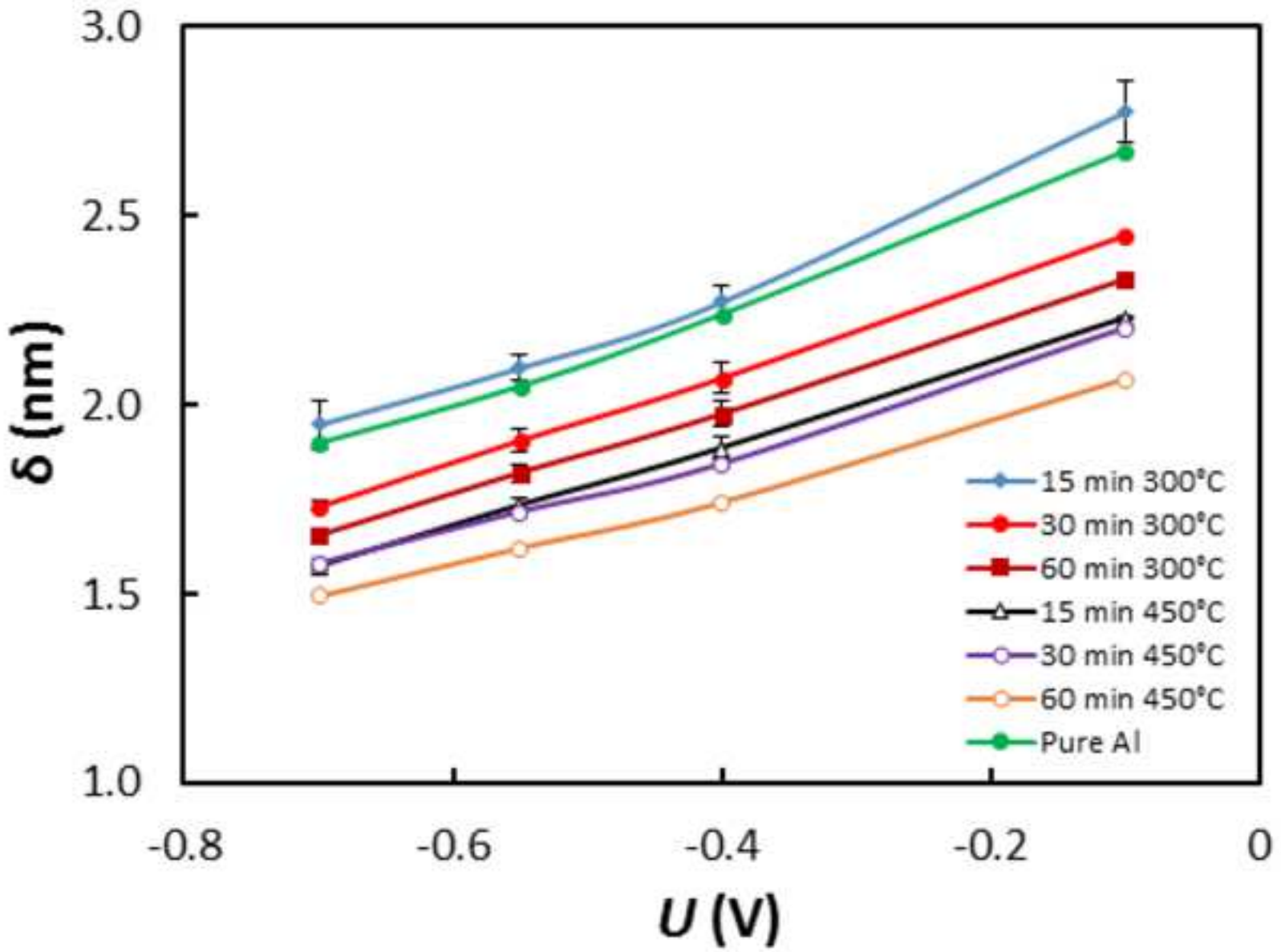

Figure 9

Click here to download Figure fig9.tif

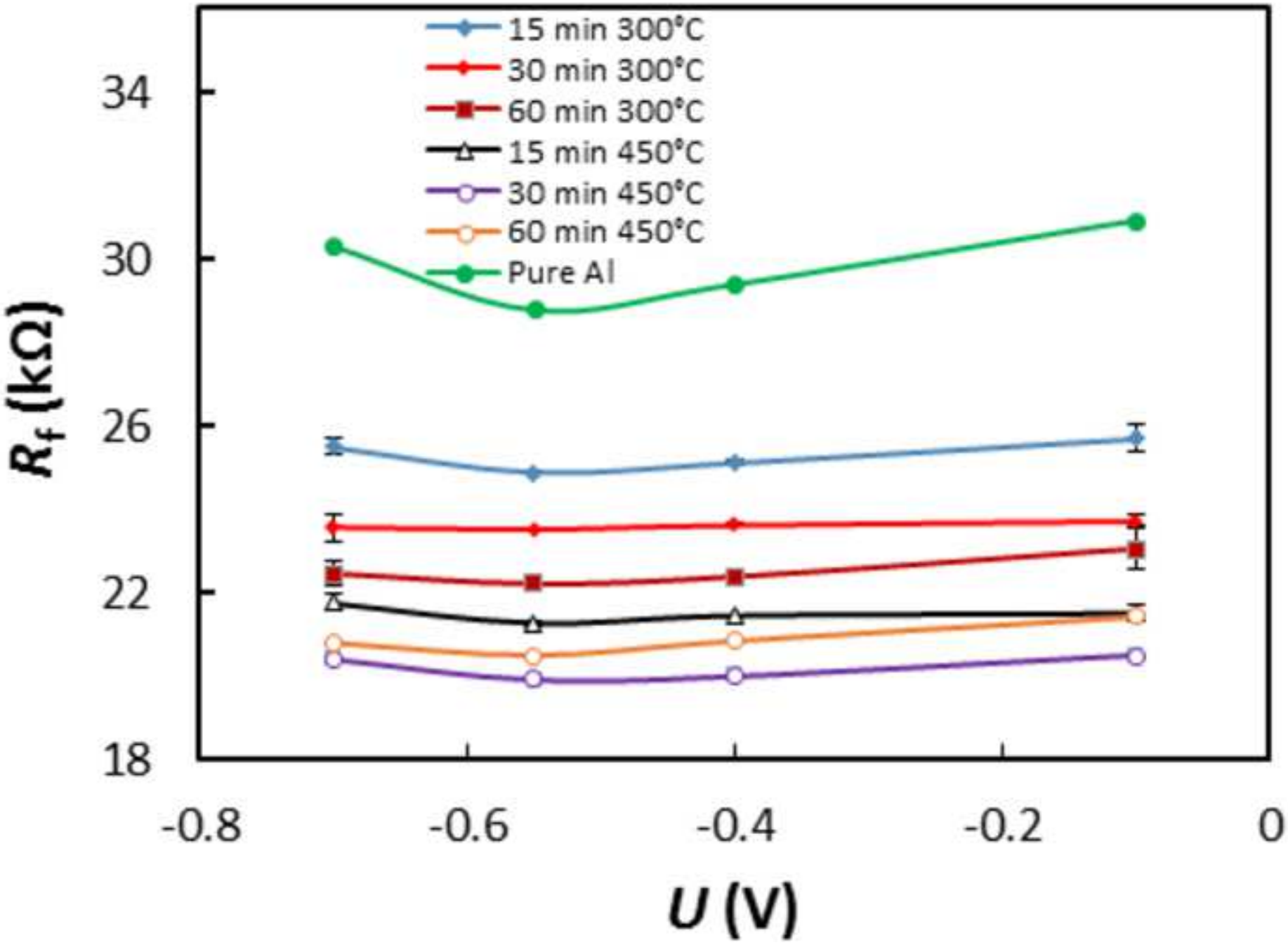

Particulate vs. continuous-film segregation of Pb at the Al-metal - thin (a few nm) oxide interface

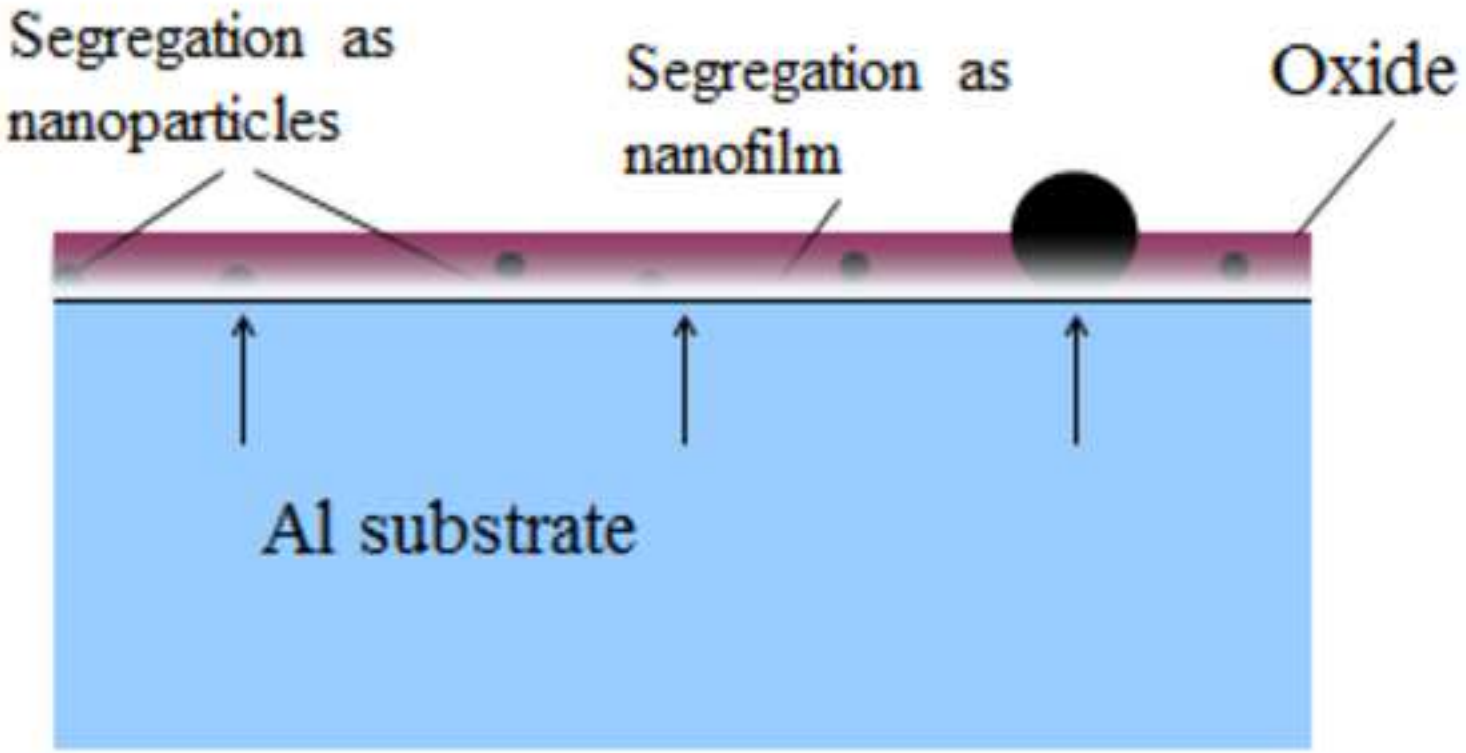

Click here to download Graphical Abstract graphical abstract.tif